Electronic Supplementary Material (ESI) for Materials Horizons.

Supporting Information

Highly efficient solar anti-icing/deicing via hierarchical structured surface

Chenyang Wu,[a,b] Hongya Geng,[b,c] Sicong Tan,[d] Jianyong Lv,[b,c] Haiqiao Wang,*[a] Zhiyuan He,*[b,c] and Jianjun Wang[b,c,e]

Table of Contents

Experimental Procedures

1.1. Materials

PDMS prepolymer (SYLGARD 184A) and thermal curing agent (SYLGARD 184B) were purchased from Dow Corning. The commercial available sugar and salt were employed to fabricate various PDMS/rGO films. Tetrahydrofuran (THF) and hydrazine monohydrate were obtained from Sigma Aldrich. All these materials were used as received without any further purification. Graphene oxide (GO) was prepared by exfoliating natural graphite by modified Hummers method.[1] Ultrapure Milli-Q water was used in all experiments.

1.2. Preparation of graphene oxide

Graphite powders (1 g) were stirred in 98% H_2SO_4 (25ml) for 2 h. Afterwards, $KMnO_4$ (2 g) was gradually added to the above suspension and the temperature was kept below 20 ^oC. The mixture was further stirred at 35^oC for 2 h and diluted with 40 ml water under vigorous stirring. 5 ml 30% H_2O_2 solution and 75 ml ultrapure water were added into the mixture. The suspension was washed with 5% HCl solution and then ultrapure water until the pH was neutralized to ~7. Finally, GO nanosheets were produced by adding 80 ml water into the precipitate and subsequently sonicated for 1 h.

1.3. Fabrication of non-templated PDMS/rGO (plane) films

The PDMS prepolymer and thermal curing agent were mixed together (10:1, w/w), a certain amount of GO dispersed in THF was added to the mixture, and then the contents were thoroughly mixed. Further, the mixture was degassed to remove the air bubbles and extra solvent before casting into a mold. The PDMS/GO film was then formed by curing at 65 °C for 3 h. GO was chemically reduced by hydrazine monohydrate at 90 °C for 2 h to obtain the PDMS/rGO film.

1.4. Fabrication of emulsion templated PDMS/rGO (EPG) film

The EPG films were prepared by the following procedures.[2] Firstly, the steps mentioned in section 1.3 were repeated to obtain the solvent free PDMS/GO mixture. Then water was added dropwise into the mixture with mechanical stirring at a speed of 600 rpm. The weight ratio of water to elastomer base was selected as 6:10. After stirring for another 5 min, the thoroughly mixed paste-like precursor was degassed and subsequently cured in an oven at 65 °C for 3 h. Afterwards, the film was chemically reduced by hydrazine monohydrate at 90 °C for 2 h. Finally, the water inside the film was evaporated in vacuum for 2 h.

1.5. Fabrication of sugar/salt templated PDMS/rGO (SPG) film

The SPG film was prepared by the following steps: the solvent-free PDMS/GO mixture was prepared, and then the mixture was subsequently poured onto the sugar/salt cubes. The prepolymer was infiltrated into the interspaces between sugar/salt particles due to the synergistic effect of capillary force and gravity. Furthermore, the mixture was cured and chemically reduced as mentioned above. At last, the sugar/salt template was removed by using hot water (90 ^oC). The size of macro structures in PDMS/rGO film was simply controlled by varying sugar/salt particles with various diameters.

1.6. Fabrication of hierarchical structured PDMS/rGO (HPG) film

Briefly, the PDMS/GO prepolymer containing emulsions was prepared first, and then the mixture was poured onto sugar/salt cubes. Furthermore, the mixture was cured and chemically reduced, afterwards the sugar/salt template was removed subsequently. Finally, the film was exposed to a vacuum condition for 2 h and followed by recovery to normal atmosphere pressure.

1.7. Characterization

The surface morphologies of PDMS/rGO films were detected by using a scanning electron microscope (SEM, JEOL-JSM-7500F, Japan). The light reflection of ultraviolet–visible (UV–vis) near infrared (NIR) spectrum was obtained by using a cary-7000 spectrometer (Agilent, USA). The solar anti-icing experiments were conducted with a solar simulator (CEL-S500, Beijing Au-light Co., Ltd., China) equipped with an optical power meter (CEL-NP2000, Beijing Au-light Co., Ltd., China) and an IR imaging camera (Tis-55, Fluke, USA). The surface structures of various PDMS/rGO films were measured by Attenuated total reflection Fourier transform infrared (ATR-FTIR) spectroscopy (Bruker TENSOR-27), Raman spectroscopy (HORIBA LabRAM HR Evolution), and X-ray photoelectron spectroscopy (XPS) (Thermofisher). Thermal conductivity measurements were carried out with the C-THERM TCI spectroscopy.

1.8. Modeling and simulation.

The heat transfer simulations were carried out with ANSYS FLUENT 6.3 software. In the modeling, the Plane, SPG-c and HPG-c films were selected as objective systems to study the temperature distribution under one sun illumination. The SADI films were placed on a thermal insulation plank (5 mm thick) with the shape parameters as follows: the film length is 150 mm; the film width is 110 mm; the film thickness is 2 mm. The incident angle is 0^{o} (q_i = 1.0 kW m^{-2}). The thermal conductivity of each sample was set the same as experimental data shown in Table S1, and the heat capacity is 1.21KJ/kg K. The initial temperature of the model is set as 300 K. The adsorption and reflectance coefficient of the films were set the same as experimental data. Solar ray tracing model was used here and only direct irradiation was considered, the photo-thermal effects of visible and infrared radiations were taken into account. The upper and surrounding boundary was set pressure-outlet boundary condition and the effect of thermal radiation, natural convection of air was considered. The governing equation of air flow and temperature fields were shown in the following:

$$\rho_0 \frac{dV}{dt} = \rho g - \nabla p + \mu \nabla^2 V \tag{1}$$

$$\rho_0 C_p \frac{dT}{dt} = \lambda \nabla^2 T + S \tag{2}$$

where μ is the air dynamic viscosity, λ is thermal conductivity, S is the source item.

Here Boussinesq approximation was applied to calculate the natural convection of air, which the density of gravity term is:

$$\rho = \rho_0 \left[1 - \alpha \left(T - T_0\right)\right] \tag{3}$$

where α is expansion coefficient, ρ_0 and T_0 are reference density and temperature respectively.

The solid film is thermal conductive inside and the substrate is heat insulating, which heat transfer can be expressed in the following equation.

$$\rho_0 C_p \frac{\partial V}{\partial t} = \lambda \nabla^2 T + q \tag{4}$$

The solar thermal effect, heat transfer and temperaure distribution on various substrates were studied. A transient simulation of 1000 s was performed on these three sets of experiments to observe the heat transfer process. Note that the thermal radiation of the illuminated films is not included in the heat transfer modeling and simulations to simplify the heat transfer model. As a result, the heating rate of simulated systems is higher than that of experiments.

1.9. IR imaging

The model of infrared camera is Fluke Tis 55 (spectral range 7.5 ~ 14 μm) with a resolution of 220×165 (Pixel^2) at a frame rate of 30 fps (accuracy: ± 2°C), the instantaneous field of view (IFOV) is 2.8 mRad. The minimum focusing distance of the IR camera is 15 cm and the noise-equivalent temperature difference is ≤0.08 °C (80 mK) when the temperature of object is 30 ^{o}C. The IR camera was mounted on a tripod and shooting in a top-down view with a controlled experimental environment. The camera was pre-calibrated before experiments. In the single droplet experiment, the temperature was calibrated with experimental data. The temperature of ice/water was measured by using both thermocouple and IR imaging camera within the range of –40 ^{o}C to 30 ^{o}C. The measurements were performed by directly dipping the thermodector into 0.5 ml water on the cryostage with the IR camera measuring the temperature at the same time. The temperature curve of ice/water measured by IR camera against temperature measured by thermodector were worked out. The temperature of ice/water on the HPG-0.3c surface was read from the IR camera and adjusted by the curve. The raw temperature data can be acquired by using Fluke Smartview 4.3 software. All the IR images are shown in 'Ironbow' color palette, and high-temperature areas are represented by bright color. Note here the temperature of ice/water obtained from IR camera was not precise especially below –15 ^{o}C and the temperature curves in Figure 4b mainly serve as guide of temperature change tendency. We have added more information into the supporting information.

1.10. Single droplet freezing experiment

The experiment was performed in a custom apparatus, consisting of a cryostage, an outside shell with thermal insulation layer, a cooling-jacket equipped with a refrigerated circulator and a thermocouple. The as-prepared HPG-0.3c film (2 mm thick films were used in all experiments) was placed on a thermal insulation foam (thickness: 3 mm) to avoid excessive rapid heat exchange between the cryostage and substrate. The temperature was regulated with the cryostage and circulating cooling-jacket, and the system temperature was double-checked with a thermocouple. As the sample reached the ambient temperature, a fixed volume of droplet (50 μL) was placed on the PDMS/rGO surface. The entire freezing process was observed by a digital single lens reflex camera (Canon 60D) mounted with a macro lens. The surface temperatures of the HPG-0.3c film and the ice/water droplet were measured by using a thermocouple and IR imaging camera. The thermocouple was attached on the surface of HPG-0.3c films. The surface temperature was tuned through 5.0 ^{o}C increment for each solar light intensity. The surface temperature near two phase boundaries were performed through 1.0 ^{o}C increment for each solar light intensity. All the data of this phase diagram were averaged from almost 30 independent events for every sample. Note here the temperature of ice/water obtained from IR camera was not precise especially below −15 ^{o}C and the temperature curves in Figure 4b mainly serve as guide of temperature change tendency.

1.11. Ice nucleation measurement

The freezing delay time (t_D) was defined as the time interval between the time when the HPG-0.3c surface reached objective temperatures and the time when freezing of water droplet atop the HPG-0.3c surface occurred. The cooling processes were regulated by a cryostage (Linkam THMS 600). The sample was placed in a thin-layer (0.2 mm) quartz box to avoid water condensation/evaporation and contaminants from the air. Quartz was used to allow maximum sunlight transmission. As the sample reached the target temperature (the surface was supercooled first), it was exposed to a certain intensity of solar illumination for at least 400 s. Afterwards, a fixed volume of water droplet (1 μL) was placed atop the HPG-0.3c surface. The freezing delay times on HPG-0.3c surface under different solar illumination intensities were measured by using a digital single lens reflex camera (Canon 60D) and a high-speed camera (Phantom v7.3) equipped with an objective lens. The time resolutions for the digital

camera and the high-speed camera were 0.167 s (60 frames s^{-1}) and 0.1 ms (10^4 frames s^{-1}), respectively. The freezing of droplets can be observed by detecting the change in opacity of droplets before and after the freezing. All the data of the freezing delay times (t_D) were averaged over 200 freezing events for each experiment. The error bars were determined by the standard errors of the mean (SEM).

1.12. Ice adhesion measurement

The ice adhesion strength was measured with a custom apparatus, consisting of a cooling stage, an XY motion stage, a force transducer, and a sample chamber.[3] Nine samples were fixed on the cooling stage with the insulation foam (thickness: 3 mm) between them to avoid over rapid heat exchange. Ice columns were formed by injecting 1 ml water into the container. Cooling of the chamber was achieved by the combined effect of cooling stage and cooling jacket. The system was kept at the testing temperature for 5 h to ensure the total freeze of the ice column. A cylindrical ice container was used similar to this report.[4] In our experiments, it can be observed that the effect of stress concentration was decreased in comparison with using a square column. The nitrogen gas was purged into the chamber in a tickle flow to minimize the effect of frost formation, as the vapor in the chamber will condense onto the sample surface and increase the measured ice adhesion. Note here the tickle flow of room temperature nitrogen gas will not strongly affect the temperature in the chamber as confirmed by the thermocouple. Quartz was used to allow maximum sunlight transmission. During the test, the force transducer was driven towards the ice column at a speed of 0.5 mm s^{-1} and the force probe was kept as close to the sample surface as possible, ≈1 mm. The peak force to detach the ice column was recorded. The resolution of the force transducers was 0.01 N. Each data of ice adhesion strength on HPG-0.3c surface at different temperatures was averaged over 10 individual measurements. Ice adhesion measurements with solar illumination were performed under solar illumination intensity of 100 mW cm^{-2}.

1.13. Simulated solar deicing experiment

The data related to average temperature and light intensity in January for six cities such as Detroit, Changchun, Saint Paul, Stockholm, Helsinki, and Snag, were acquired from NASA Prediction of Worldwide Energy Resources (NASA POWER, https://power.larc.nasa.gov/). The data was collected from 30-year (from January 1984 to December 2013) meteorological solar monthly and annual climatologies. Average light intensities (daytime) in January were calculated by multiplying average daylight hours and direct normal radiation (average light intensities during day and night). Experiments were performed under simulated environments in the laboratory. For all experiments, the films were weighed before and after covered with frost to calculate the weight of frost. The change in frost coverage was recorded by using a digital camera, and further analysed by using imageJ software. Simulation of frost, rime, and glaze accumulation were performed as follows: (a) Frost: HPG-0.3c films were placed atop dry ice (−78 °C) to accumulate frost on the surface for 5 min (RH = 45%, thickness of frost at about 2 mm); (b) Rime: The films were put on the cooling stage inside a closed chamber with a humidifier and an air fan. The temperature of the cooling stage was −12 °C and the RH in the chamber was 100%. The wind speed in the chamber was about 2 m/s. Ambient temperature in the chamber was about −30 °C to create supercooled water droplet in the air. After 12 min, the thickness of rime on the HPG-0.3c surface was about 2 mm; (c) Glaze: In a similar setup, the RH in the chamber was 100% and impacting of supercooled water to the surface can be observed. While the temperature of cooling stage was set to −4 °C with no wind blowing. The thickness of glaze accumulated on the surface was about 1 mm after 15 min.

1.14. Calculation of ice removing rate and energy efficiency

The experimental value of ice removing rate was simply calculated by using the following equation:

$$v_{melt} = \frac{dm_i}{A \times dt} \tag{5}$$

where m_i is the mass of ice on the surface, A denotes the projected surface area, and t is the time for the ice melting/removing.

The energy conversion efficiency of η_{sl} is defined as the ratio of energy consumed by the ice melting process to the total energy input. Then the energy conversion efficiency can be obtained by using the following equation:

$$\eta_{sl} = \frac{C \times dm_i \times (T_0 - T) + \Delta H_{fus} \times dm_i}{q_{in} \times A \times dt} \tag{6}$$

where C is the heat capacity of ice, T_0 denotes the initial temperature of frost, and T represents melting temperature of ice. ΔH_{fus} is enthalpy of ice melting and q_{in} is intensity of solar illumination.

Substituting Eq. (5) into (6), η_{sl} can be written as follows:

$$\eta_{sl} = \frac{C \times (T_0 - T) + \Delta H_{fus}}{q_{in} \times A} \times v_{melt} \tag{7}$$

Table S1. Thermal conductivities of all films with 0.3 wt% rGO contents.

Sample	Thermal conductivity [W m^{-1} K^{-1}]
Plane	0.221
EPG	0.164
SPG-a	0.069
SPG-b	0.057
SPG-c	0.045
HPG-a	0.068
HPG-b	0.059
HPG-c	0.043

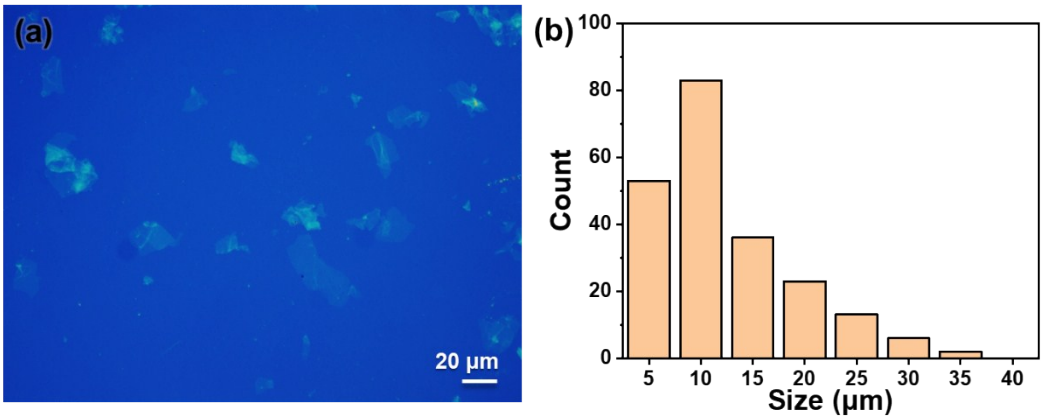

Figure S1. (a) Optical microscopy image and (b) corresponding size distribution histogram of GO nanosheets. The histogram of GO size distribution was obtained based on more than 200 measurements.

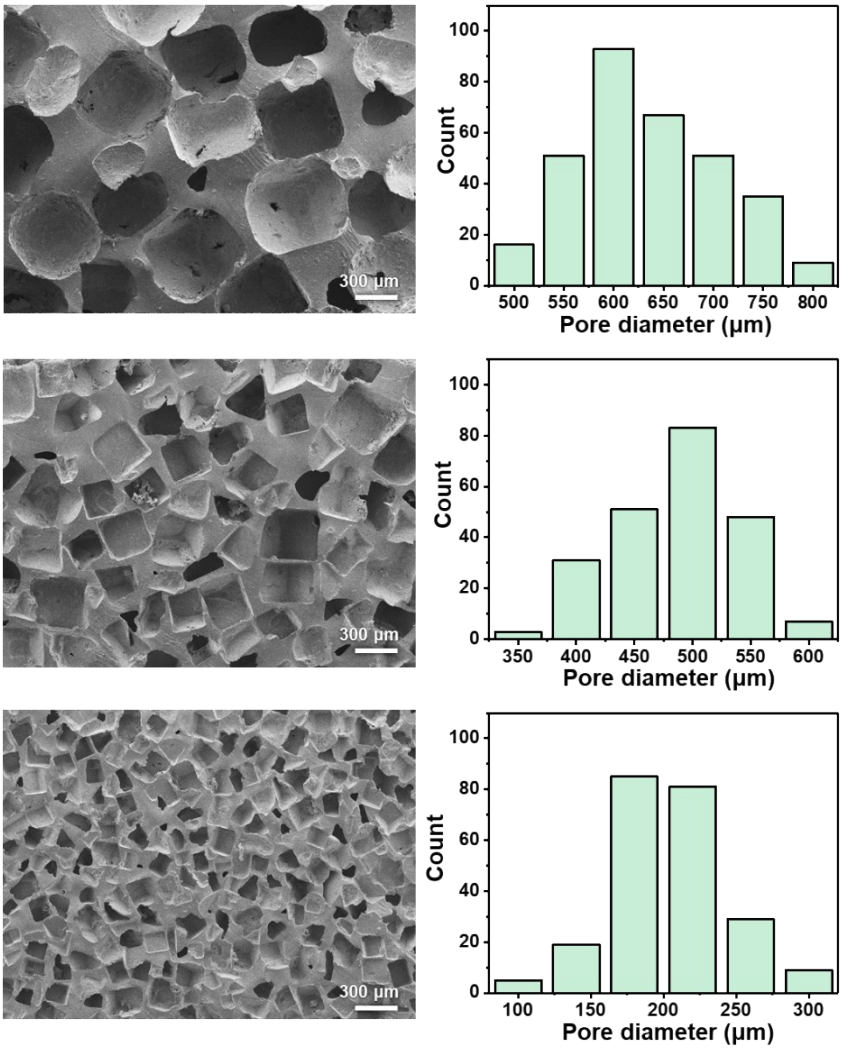

Figure S2. SEM images of HPG films fabricated via dual-templated methods by simply changing sugar/salt particle diametres (left column), and corresponding histograms of size distribution of different macro-structures (right column). From top to bottom: HPG-a, HPG-b, and HPG-c films. The histograms of size distribution of different macro-structures were obtained after more than 200 measurements.

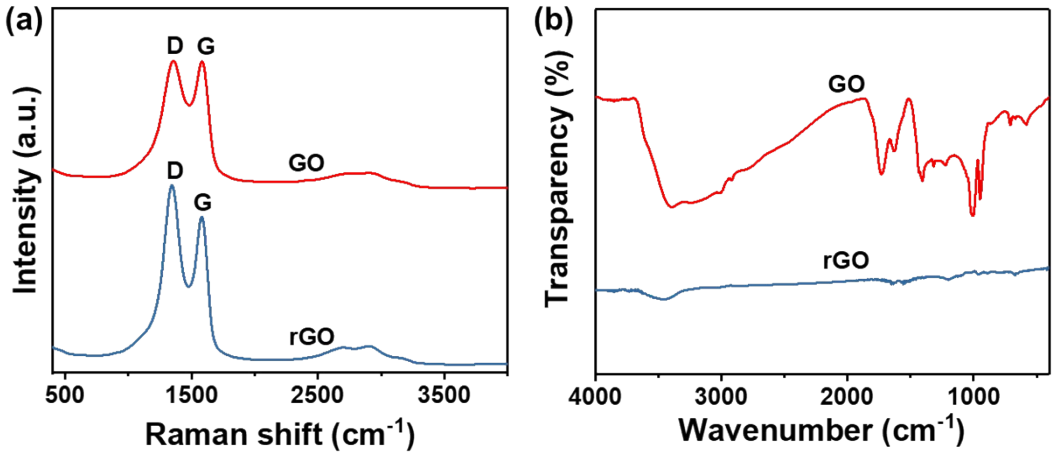

Figure S3. (a) Raman, and (b) FTIR spectra of GO and rGO.

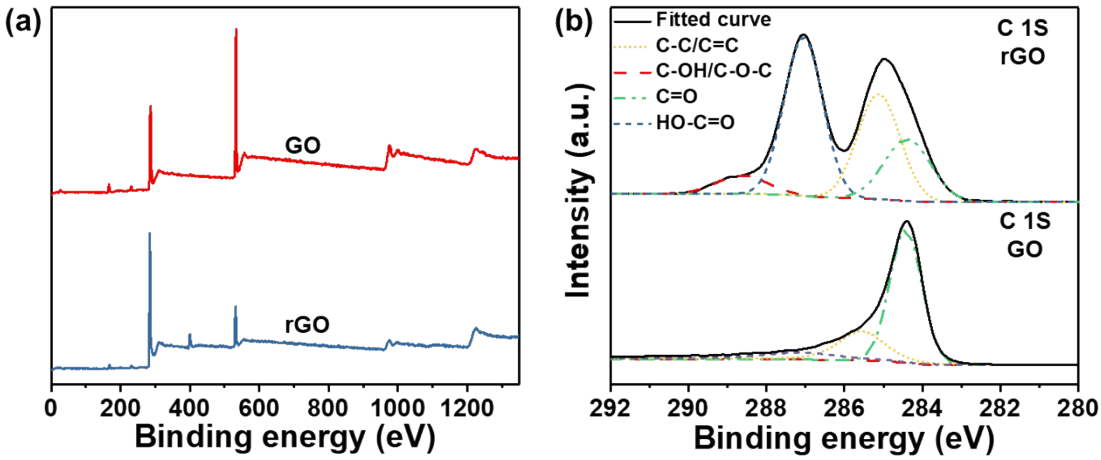

Figure S4. (a) XPS measurements, and (b) C1s XPS spectra of GO and rGO.

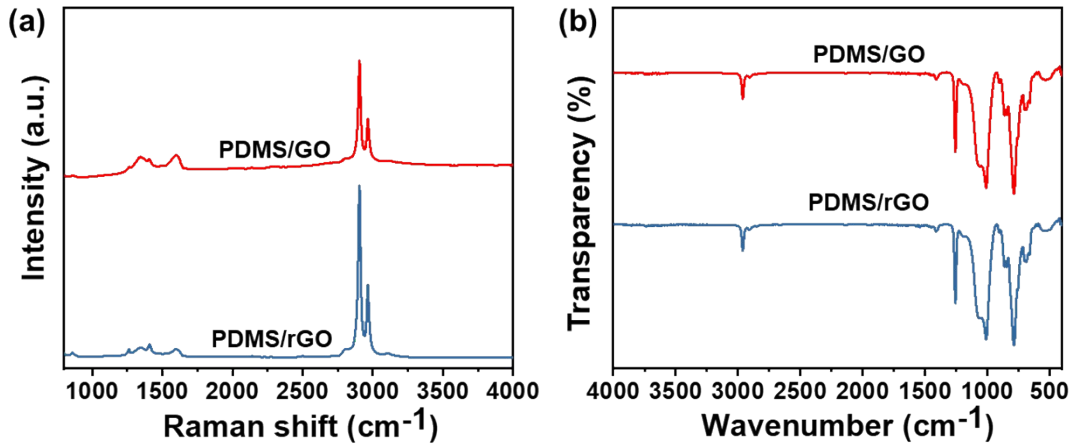

Figure S5. (a) Raman, and (b) FTIR spectra of PDMS/GO and PDMS/rGO.

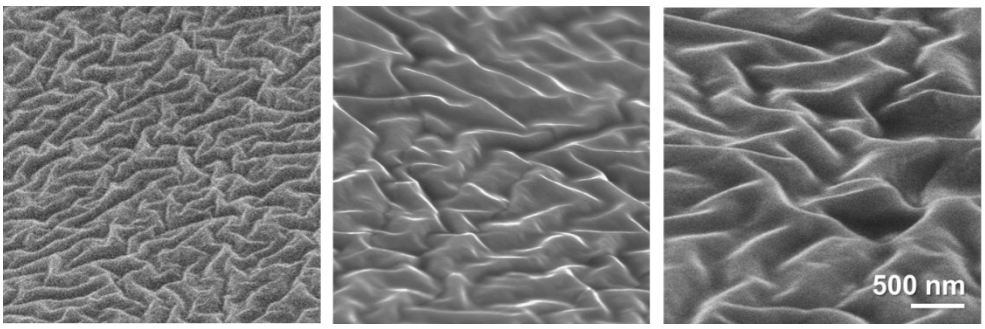

Figure S6. SEM images of varied sizes of wrinkles ranging from 128 to 320 nm. The mean size of wrinkles were measured in 10 locations for over 200 times in each sample.

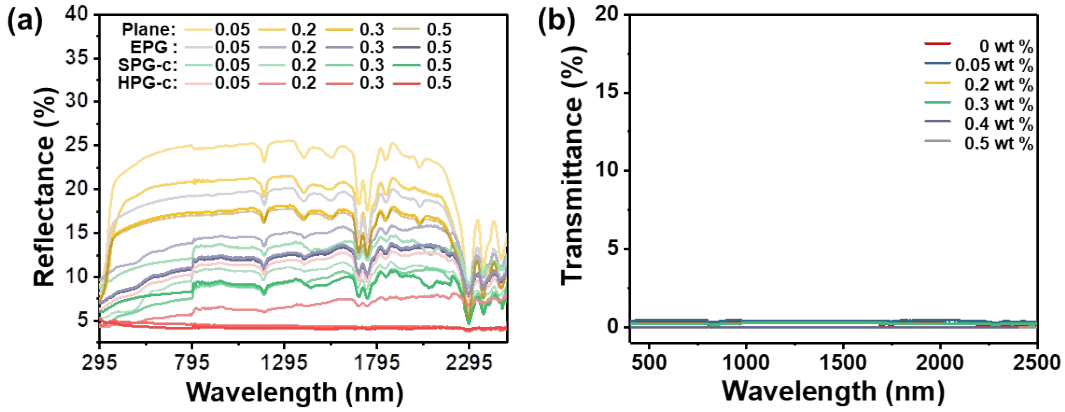

Figure S7. (a) Reflectance of films based on different fabrication methods with various rGO contents in UV–Vis–NIR spectrum; (b) Transmittance of HPG-c films containing various rGO contents in UV–Vis–NIR spectrum.

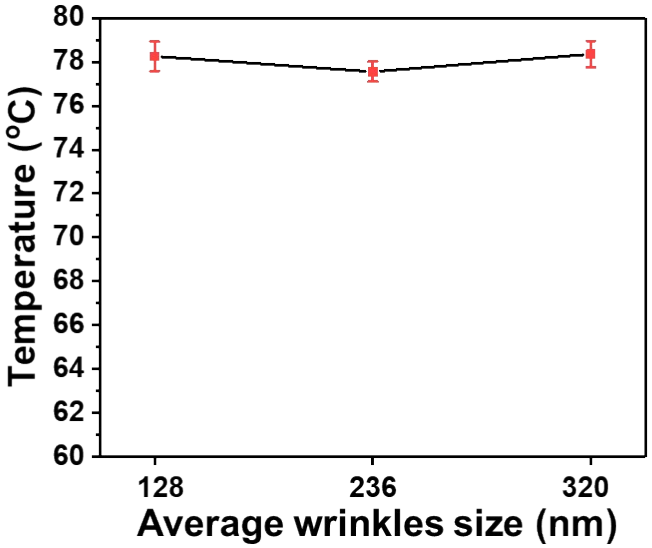

Figure S8. HPG-0.3c samples with various average wrinkles size under solar illumination of 1.0 kW m^{-2} for 400 s.

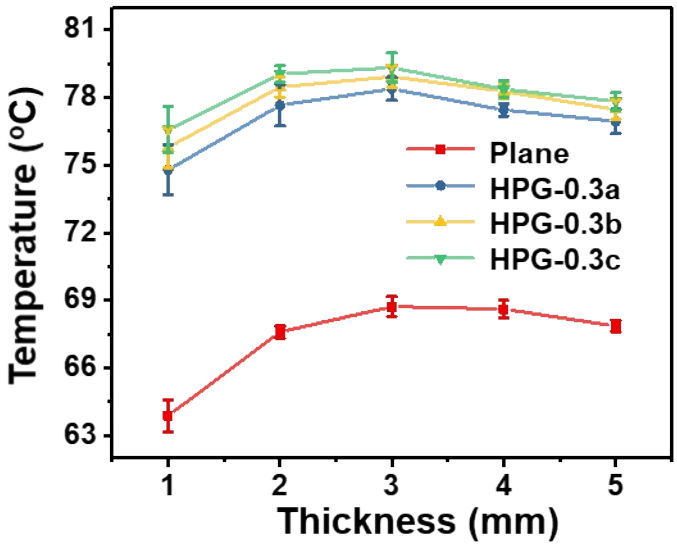

Figure S9. Steady state surface temperature of all samples with various thickness under one sun illumination for 400 s. The ambient temperature is 25 °C. Taking the HPG film (with a width of ca. 15 cm and a length of ca. 10 cm) as an example, the lateral area of heat radiating increases 5 cm^2 with the increase of thickness of 1 mm. When the thickness exceeds 3 mm, the equilibrium temperature will decrease due to enhanced heat radiating from the lateral area.

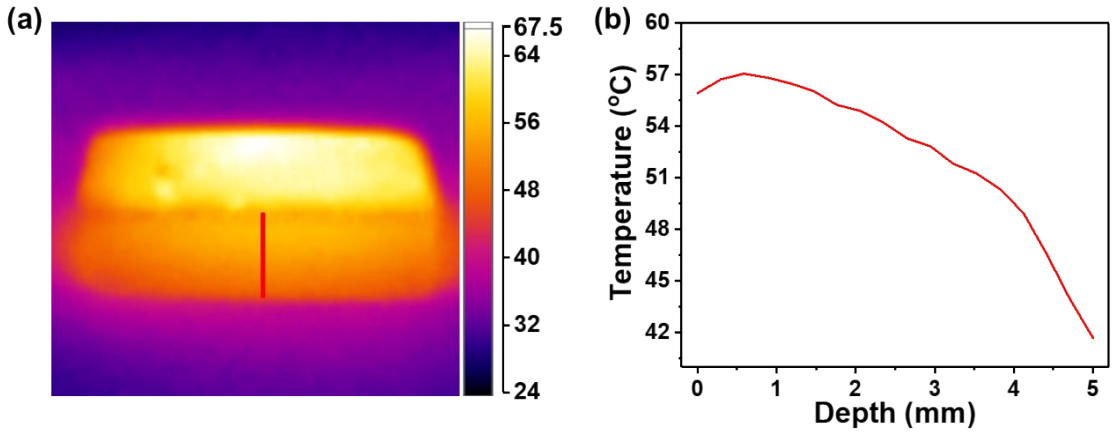

Figure S10. (a) IR images (side view) of HPG-0.3c film (thickness: 5 mm) under solar illumination for 400 s. (b) The vertical temperature distribution of the HPG-0.3c film along the red line from up to bottom.

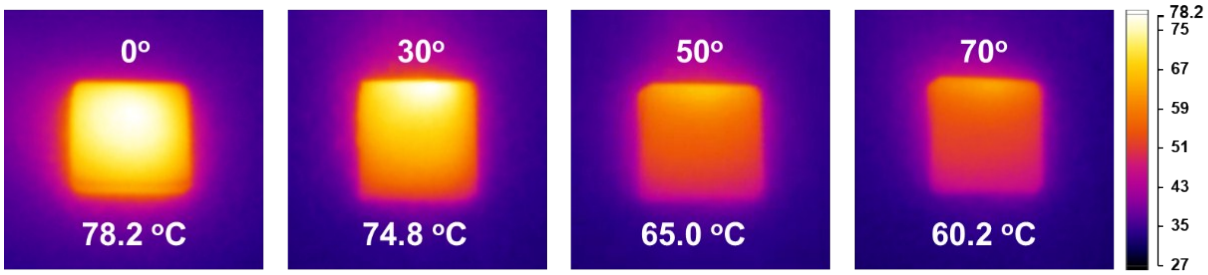

Figure S11. IR images of HPG-0.3c films under various incident angles for 400 s (q_i = 1.0 kW m^{-2}).

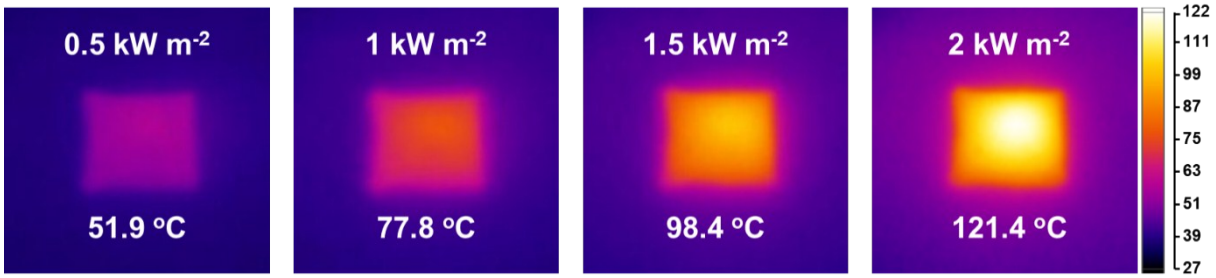

Figure S12. IR images of HPG-0.3c films under various illumination intensities for 400 s.

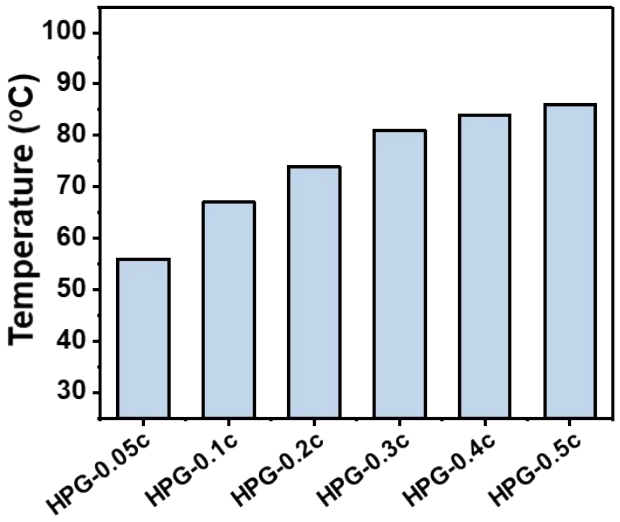

Figure S13. Simulated equilibrium temperatures of HPG-c films with various rGO content under one sun illumination.

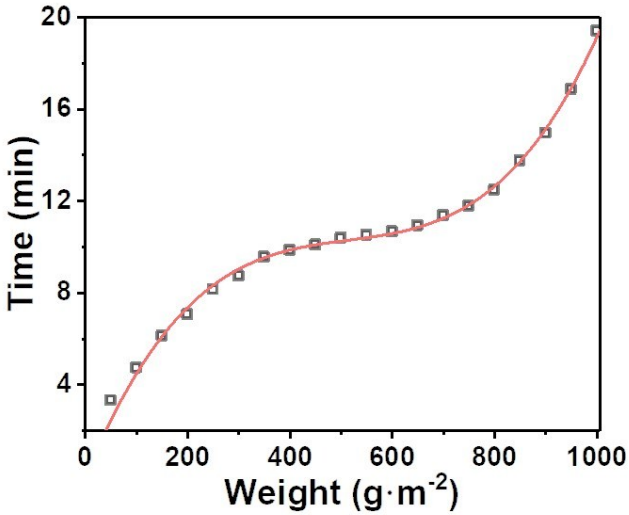

Figure S14. Ice removing time as a function of covered ice weight on HPG-0.3c film at −35 °C (q_i = 1.0 kW m^{-2}).

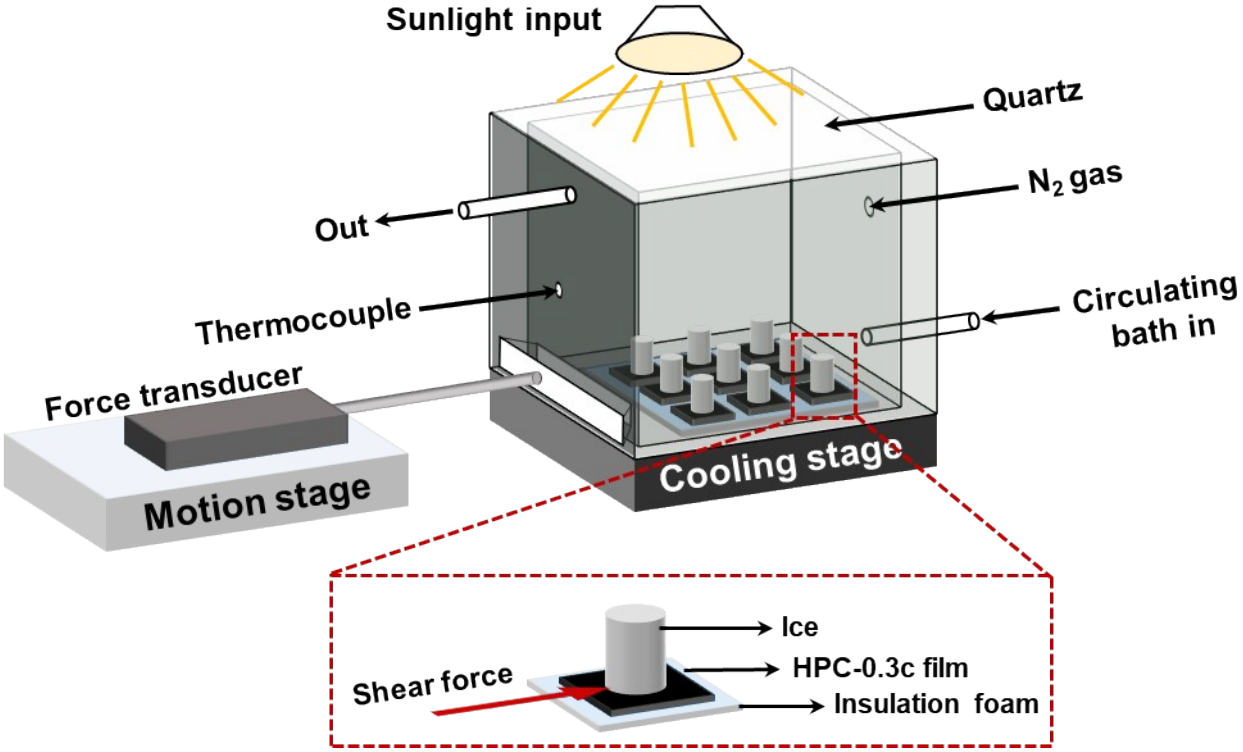

Figure S15. Illustration of ice adhesion measurment in shear mode under sunlight illumination.

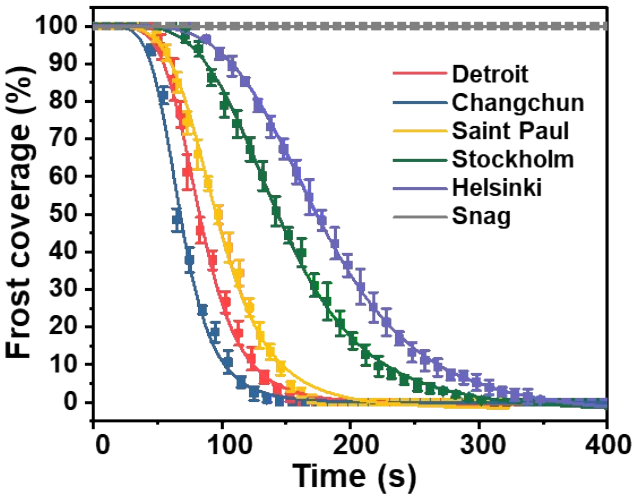

Figure S16. Solar deicing experiments performed under different simulated environments of six typical cities.

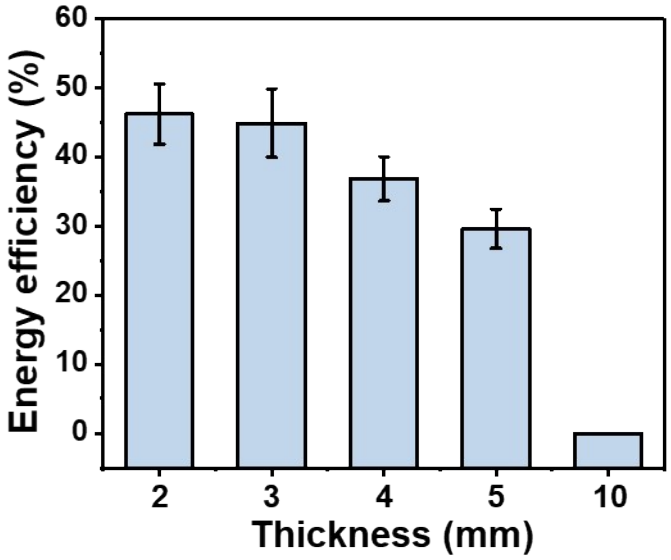

Figure S17. Deicing efficiency under simulated realistic environment of Changchun with various ice thicknesses on HPG-0.3c films. As the ice thickness increases from 2 to 10 mm, the deicing efficiency decreases gradually, and the efficiency drops to zero when the ice thickness is 10 mm. Because the ice itself can reflect or absorb part of the solar energy, and the energy efficiency decreases with increase of ice thickness. When the ice thickness increases to 10 mm, there is not enough sunlight to reach the SADI surface. As a result, the atop ice cannot be melted, and the deicing efficiency is calculated as zero.

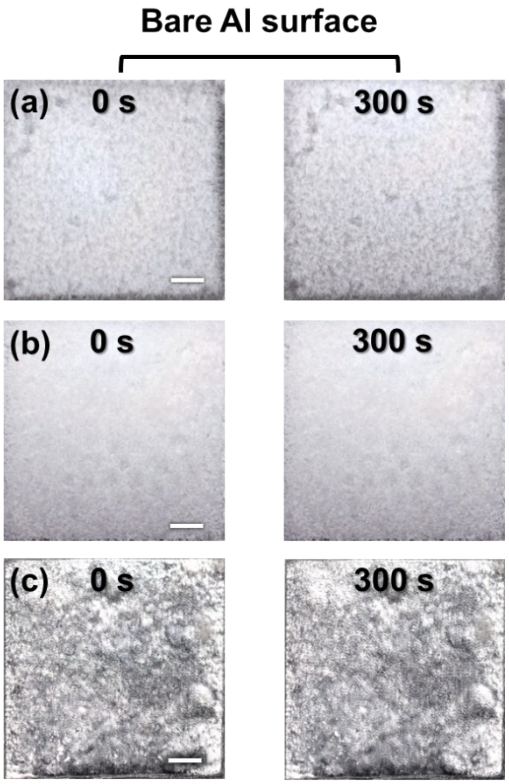

Figure S18. Bare aluminum surfaces covered with (a) frost, (b) rime and (c) glaze at −17.3 °C under solar illumination of 608 W m^{-2} for 300 s. The scale bar is 300 μm**.**

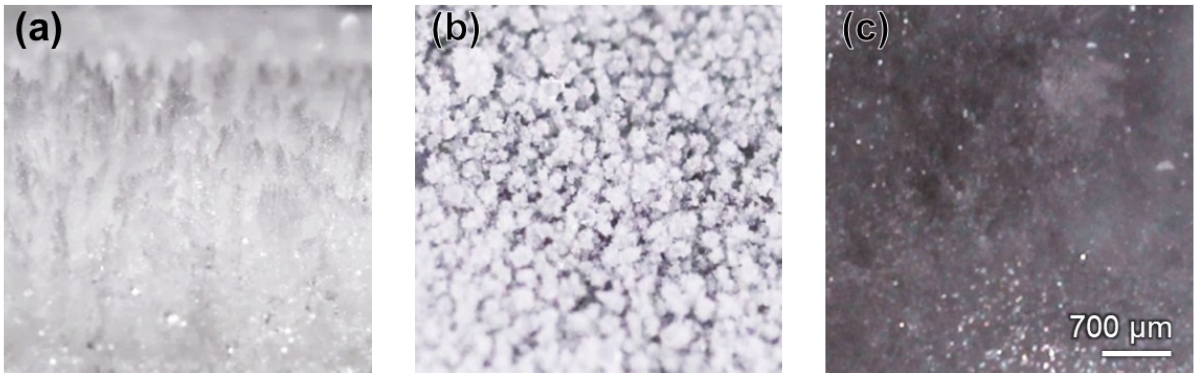

Figure S19. Magnified optical images of (a) frost, (b) rime and (c) glaze covered on HPG-0.3c films. The morphology of three icing conditions are shown here, as there is much difference among them in the optical properties and densities.

References

[1] K. Krishnamoorthy, M. Veerapandian, K. Yun, S. J. Kim, *Carbon* **2013**, *53*, 38-49.
[2] A. Davis, S. Surdo, G. Caputo, I. S. Bayer, A. Athanassiou, *ACS Appl. Mater. Interfaces* **2018**, *10*, 2907-2917.
[3] Y. Wang, X. Yao, S. Wu, Q. Li, J. Lv, J. Wang, L. Jiang, *Advanced Materials* **2017**, *29*, 1700865.
[4] Z. He, Y. Zhuo, J. He, Z. Zhang, *Soft Matter* **2018**, *14*, 4846-4851.